<u>Responses to the Manuscript essd-2022-83 RC3</u>:

A global dataset of spatiotemporally seamless daily mean land surface temperatures: generation, validation, and analysis

Dear reviewer #3,

The authors would like to thank you for providing us with thoughtful and outstanding comments. We have addressed all comments in detail and revised the manuscript accordingly and tracked the changes so that you can see that we have rewritten many parts of the manuscript. Point-by-point responses are provided below.

Yours sincerely,

Falu Hong, Wenfeng Zhan*, Frank-M. Göttsche, Zihan Liu, Pan Dong, Huyan Fu, Fan Huang, and Xiaodong Zhang

Email: zhanwenfeng@nju.edu.cn

I. TABLE OF CONTENTS

II. ATTENTIONS

(1) In the following responses, texts contained within the red braces {…} are identical to those in our revised manuscript.

(2) In the following responses, the line numbers [Line XXX-XXX] refer to the clean version of the revised manuscript.

(3) Fig. 1, 2, and 3…, and Eq. 1, 2, and 3… refer to the figures and equations excerpted from our revised manuscript.

(4) In the following responses, all the related references are provided collectively in Part IV References.

III. RESPONSES TO REVIEWER #3

Comment #1

spatiotemporally seamless land surface temperature at daily, monthly, and yearly scales are important for LST-related researches. This study presents a meaningful study with the use of MODIS LST product and reanalysis data to generate the mean LST value at different scales. It was well organized and the results were with good accuracy. Overall, the manuscript can be accepted with minor revision:

Authors' reply:

Thanks for your appreciation. The point-to-point responses are given as follows.

Comment #2

There are many other reanalysis data available and why you choose the MERRA2 dataset? What is advantage of this dataset?

Authors' reply:

Thanks for your comment. We agree with you that there are many other reanalysis data, such as ERA-land (Muñoz-Sabater et al., 2021), GLDAS (Rodell et al., 2004), JRA-55 (Kobayashi et al., 2015), and NCEP (Kalnay et al., 1996) reanalysis datasets. We chose MERRA2 dataset because it can provide global hourly air temperature. The MERRA2 air temperature can provide the annual air temperature variation pattern to simulate LST fluctuations induced by synoptic conditions. This information is used in the ATC model to reconstruct the under-cloud LSTs at four overpassing times. Other reanalysis datasets can replace the MERRA2 dataset if they could provide similar information.

Comment #3

The key steps are suggested to be clarified in in figure 2. The pre-processing is not included in this flowchart.

Authors' reply:

Thanks for your comment. We have added the preprocessing steps which include unifying the projection system and resampling the datasets to the same spatial resolution in the flowchart. The revised flowchart is given as follows for your convenience.

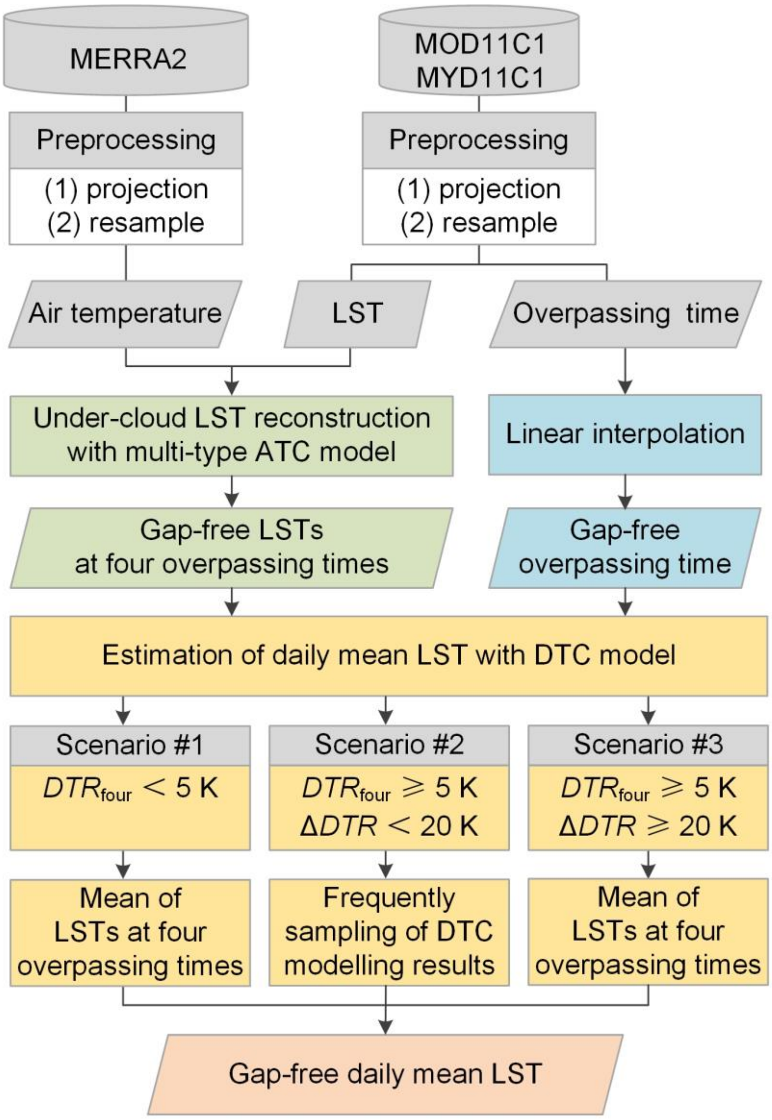

Fig. 1. Flowchart of the IADTC framework. *DTR_{four}* refers to diurnal temperature range (DTR) calculated as the maximum minus the minimum from the gap-free LSTs at the four overpassing times; *DTR_{DTC}* refers to the DTR calculated from the hourly LSTs modelled with the DTC model. Δ*DTR* refers to the absolute difference between *DTR_{four}* and *DTR_{DTC}*.

Comment #4

175: A basic equation of the single-type and multi-type model is better to be provided here.

Comment #5

Figure 3: multi-type ATC models are identical? Why there is no differences? It will be

a little confused on the naming of the ATC models for single or multi-type model and single or double-sinusoidal ATC model?

Authors' reply:

Thanks for your comment. Comments #4 and #5 are both related to descriptions of ATC model, so we combine the response. We agree with you that some of the ATC model descriptions are redundant and could be misleading.

We summarized the basic equation of ATC model as Eq. R1. For the single-type ATC model, M equals 1 for the global application, i.e., the single-sinusoidal version was applied to the global scale. As for the multi-type ATC model, the value of M is different at different latitude zones. In low-latitude (23.5° N – 23.5° S) and high-latitude regions (66.5° N/S – 90° N/S), M equals 2, i.e., the double-sinusoidal version was applied to these regions. In mid-latitude regions (23.5° N/S – 66.5° N/S), M equals 1, i.e., single-sinusoidal version was used.

To address your question about the identical results between the single-type and multi-type ATC models, the results of single-type and multi-type ATC models are identical in mid-latitude region because they both use the single-sinusoidal version (M = 1). Therefore, the results in Fig. 3b are identical. While the results of single-type and multi-type ATC models are different in low-latitude and high-latitude regions (Fig. 3a & Fig. 3c) because the single-type ATC model still uses the single-sinusoidal version (M =1) while the multi-type ATC model use the double-sinusoidal version (M = 2).

$$\begin{cases} T_{\mathrm{ATCM}}(d) = T_0 + \sum_{m=1}^{M} A_{\mathrm{m}} \, sin\left(\frac{2\pi m d}{N} + \theta_{\mathrm{m}}\right) + k \cdot \Delta T_{\mathrm{air}}(d) \\ \Delta T_{\mathrm{air}}(d) = T_{\mathrm{air}}(d) - T_{\mathrm{ATCO}}(d) \\ T_{\mathrm{ATCO}}(d) = T_0{}' + \sum_{m=1}^{n} A'_{\mathrm{m}} sin\left(\frac{2\pi m d}{N} + \theta'_{\mathrm{m}}\right) \end{cases} \qquad \text{Eq. R1}$$

where $T_{\mathrm{ATCM}}(d)$ denotes the daily LST variations simulated with the ATC model; M is the number of used harmonic components; d and N are the day of year (DOY) and number of days in a year, respectively; $\Delta T_{\mathrm{air}}(d)$ is the difference between the daily SATs (i.e., $T_{\mathrm{air}}(d)$, obtained from MERRA2 reanalysis data) and the modelled air temperatures with the original ATC model ($T_{\mathrm{ATCO}}(d)$); and T_0, A_{m}, θ_{m}, and k are the parameters that need to be solved with the cloud-free daily LSTs and SATs, usually through the least-square method.

To reduce the redundancy and clarify the description, we have revised Section 3.1.2. The revised version is given as follows for your convenience.

3.1.2 Under-cloud LST reconstruction with multi-type ATC model

The general formula of ATC model is displayed in Eq. 2. The single-type ATC model in the OADTC framework uses a single sinusoidal function (M = 1 in Eq. 2) to model the intra-annual LST variations driven by solar radiation change and incorporates surface air temperatures to help simulate the LST fluctuations induced by synoptic conditions (Zou et al., 2018; Liu et al., 2019b). The use of a single sinusoidal function is generally acceptable for mid-latitude regions. However, a single sinusoidal is no longer suitable for low-latitude because there are two solar radiation peaks within a yearly cycle over low-latitude regions (Xing et al., 2020; Bechtel, 2015; Cao and Sanchez-Azofeifa, 2017); it is also inadequate for high-latitude regions where polar days and nights occur (Østby et al., 2014; Liu et al., 2019; Westermann et al., 2012). Therefore, the use of the single-type ATC model in the OADTC framework is less suitable to generate T_{dm} at the global scale (Fig. 2). To overcome this limitation, the IADTC framework uses different versions of ATC model (termed the multi-type ATC model) to reconstruct under-cloud LSTs over the low-, mid-, and high-latitude regions, respectively. The details are given as follows:

(1) Low-latitude regions (23.5° N – 23.5° S)

The solar radiation possesses two peaks within a yearly cycle over low-latitude regions (Fig. 2a). We therefore employed the ATC model with two sinusoidal functions *(*M = 2 in Eq. 2*)* to reconstruct the daily LST dynamics within an annual cycle (Liu et al., 2019b; Xing et al., 2020).

(2) Mid-latitude regions (23.5° N/S – 66.5° N/S)

The solar radiation peaks once in summer during an annual cycle. We therefore employed the ATC model with single-sinusoidal function *(*M = 1 in Eq. 2*)* to reconstruct the daily LST dynamics (Fig. 2b).

(3) High-latitude regions (66.5° N/S – 90° N/S)

The polar day/night phenomena occur over high-latitude regions and the duration increases with the latitude. Theoretically, over these regions, the ATC model with multiple sinusoidal functions should be the best choice. However, the number of cloud-free MODIS observations is limited, and additional model complexity can lead to over-fitting and weaken the generalization ability of the ATC model (Liu et al., 2019b). To balance model accuracy and generalization ability, the ATC model with two sinusoidal functions was selected for high-latitude regions (see Fig. 2c).

$$
\begin{cases}
T_{\mathrm{ATCM}}(d) = T_0 + \sum_{m=1}^{M} A_{\mathrm{m}} \sin\left(\frac{2\pi m d}{N} + \theta_{\mathrm{m}}\right) + k \cdot \Delta T_{\mathrm{air}}(d) \\
\Delta T_{\mathrm{air}}(d) = T_{\mathrm{air}}(d) - T_{\mathrm{ATCO}}(d) \\
T_{\mathrm{ATCO}}(d) = T_0{'} + \sum_{m=1}^{M} A_{\mathrm{m}}^{'} \sin\left(\frac{2\pi m d}{N} + \theta_{\mathrm{m}}^{'}\right)
\end{cases}
\tag{2}
$$

where $T_{\mathrm{ATCM}}(d)$ denotes the daily LST variations simulated with the ATC model; M is the number of used harmonic components; d and N are the day of year (DOY) and number of days in a year, respectively; $\Delta T_{\mathrm{air}}(\mathrm{d})$ is the difference between the daily SATs (i.e., $T_{\mathrm{air}}(\mathrm{d})$, obtained from MERRA2 reanalysis data) and the modelled air temperatures with the original ATC model ($T_{\mathrm{ATCO}}(d)$); and T_0, A_{m}, θ_{m}, and k are the parameters that need to be solved with the cloud-free daily LSTs and SATs, usually through the least-square method.

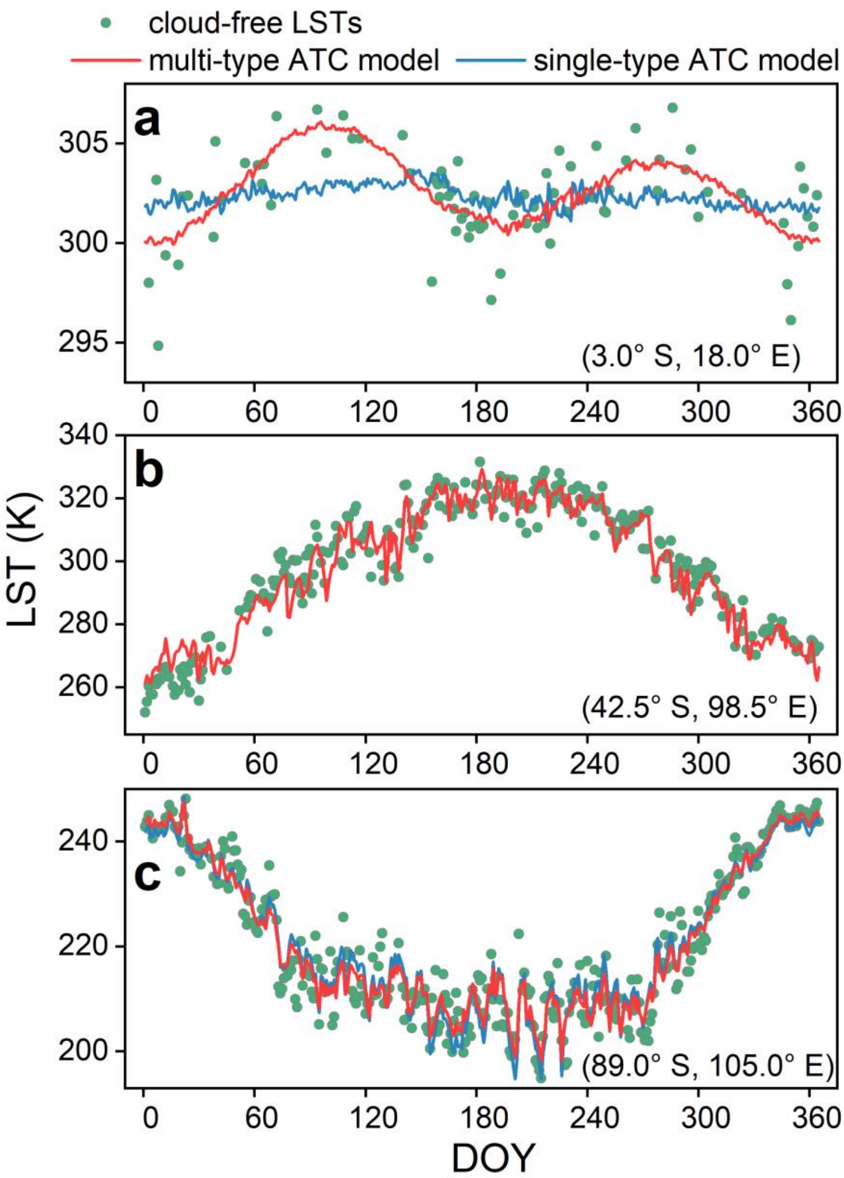

Fig. 2. Comparison of reconstructing under-cloud LSTs with multi-type and

single-type ATC models at different latitudes. (a), (b), and (c) show three examples of ATC modelling at low-, mid-, and high-latitudes for cloud-free Terra-day LST in 2019. The green circles, blue lines, and red lines denote the cloud-free observations and LSTs simulated by the single- and multi-type ATC models, respectively. Note that for (b) the results of the single- and multi-type ATC models are identical since they both use the ATC model with single-sinusoidal function.

Comment #6

Section 3.1.3: I think it should be the interpolation of the missing LSTs but not overpassing times.

Authors' reply:

Thanks for your comment. Section 3.1.2 is the under-cloud LST reconstruction and Section 3.1.3 is the interpolation of overpassing time. The interpolation of overpassing time is required because, in the original MODIS LST products (MOD11C1 and MYD11C1), not only the cloud contaminated LSTs are missing, but also the overpassing time of the cloud contaminated pixel. Because the overpassing time is synchronically masked with the cloud contaminated LST. The overpassing time is the required input variable in the DTC model, and the missing overpassing time cannot drive the DTC model. Therefore, we used linear interpolation to reconstruct the missing overpassing time, which is the content of Section 3.1.3.

Comment #7

Actually, the DTC model should be not applied to get the DTCdm when there are cloud-cover observations.

Authors' reply:

Thanks for your comment. Although the current DTC model is designed for the clear-sky condition, it can be applied to estimate daily mean LST (T_{dm}) with acceptable accuracy. This has been validated by our previous study (Hong et al., 2021). We acknowledge that under cloudy conditions, the DTC-modelled diurnal LST dynamics (blue and red lines in Fig. R1) could have significant deviations compared with the actual diurnal LST dynamics (black line in Fig. R1). However, the aggregated T_{dm} can still achieve satisfactory accuracy (Hong et al., 2021) because: (1)

the positive and negative biases of the modelled diurnal LST dynamic were partly offset when calculating the daily mean LST; (2) under cloudy condition, the diurnal LST variation is relatively mild, which can also reduce the daily mean LST estimation error to some degree.

In this paper, we also validated the accuracy of T_{dm} estimated with the DTC model. For the SURFRAD datasets, the MAEs of estimated T_{dm} at the daily and monthly scales are 1.4 K and 0.6 K, respectively (Fig. 6). For the FLUXNET datasets, the MAEs of T_{dm} are 1.1 K and 0.5 K at the daily and monthly scales, respectively (Fig. 7). The validation results show that the DTC model can be applied to estimate daily mean LST under cloudy conditions.

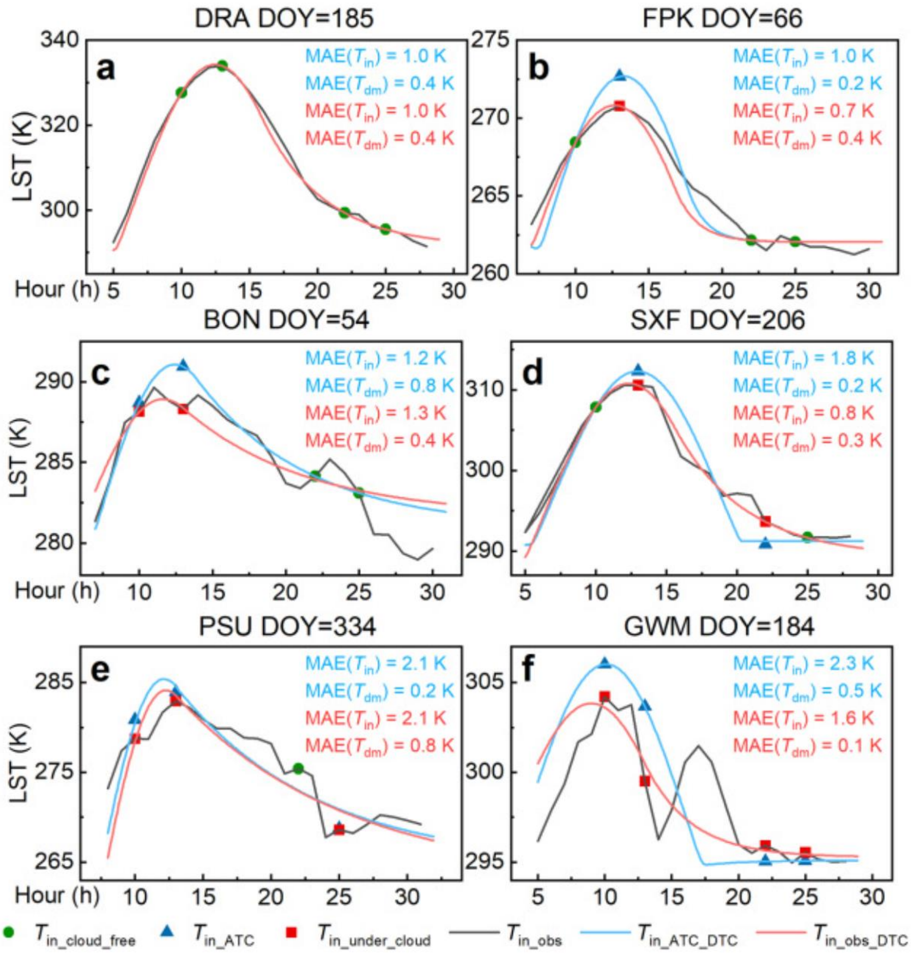

Download : Download high-res image (642KB)   Download : Download full-size image

Fig. 12. Typical examples of DTC modelling results obtained for six SURFRAD sites in 2017. The blue (red) numbers in the upper right corners provide the MAEs of $T_{\text{in\_ATC\_DTC}}$ and $T_{\text{dm\_ATC\_DTC}}$ ($T_{\text{in\_obs\_DTC}}$ and $T_{\text{dm\_obs\_DTC}}$). In (a), the conditions are completely cloud-free: therefore, the results for $T_{\text{in\_ATC\_DTC}}$ and $T_{\text{in\_obs\_DTC}}$ are identical (i.e., ATC modelling is not needed). (b)-(f) represent the cases with increasing cloud contamination. (For interpretation of the references to colour in this figure legend, the reader is referred to the web version of this article.)

Fig. R1. Screenshot of Fig. 12 in Hong et al. (2021).

Comment #8

Besides the direct validation of the estimated mean values at different temporal scales, there is a lack of the evaluation of the reliability of the trend detection based on the generated dataset. How about the performance of the dataset on identifying the area with significant trends.

Authors' reply:

Thanks for your comment. To evaluate the reliability of the LST trend based on the generated daily mean LST, ground truth is required. The LST trend calculated based on the *in situ* measurement is sensitive to the local climate variation, and there is a scale mismatch between the site-level LST trend and pixel-level LST trend. Therefore, the LST trend based on the *in situ* measurement might not be representative to evaluate the LST trend based on the generated daily mean LST dataset.

Acquiring the ground truth to validate the generated daily mean LST product could be costly and complicated. Consequently, to evaluate the reliability of the LST trend detection based on the generated GADTC dataset, we compare the LST trend based on generated GADTC products with other studies. We found that the LST trend detected based on the generated GADTC products (Fig. 10) is similar to the previous studies conducted by Sobrino et al. (2020) (Fig. R2) and Mao et al. (2017) (Fig. R3). Additionally, we provided the LST anomalies from 2003 to 2019 of each continent and global scale (Fig. R4). Fig. 10 and Fig. R4 both confirm the significant trends in certain areas, such as the warming and Europe and Arctic.

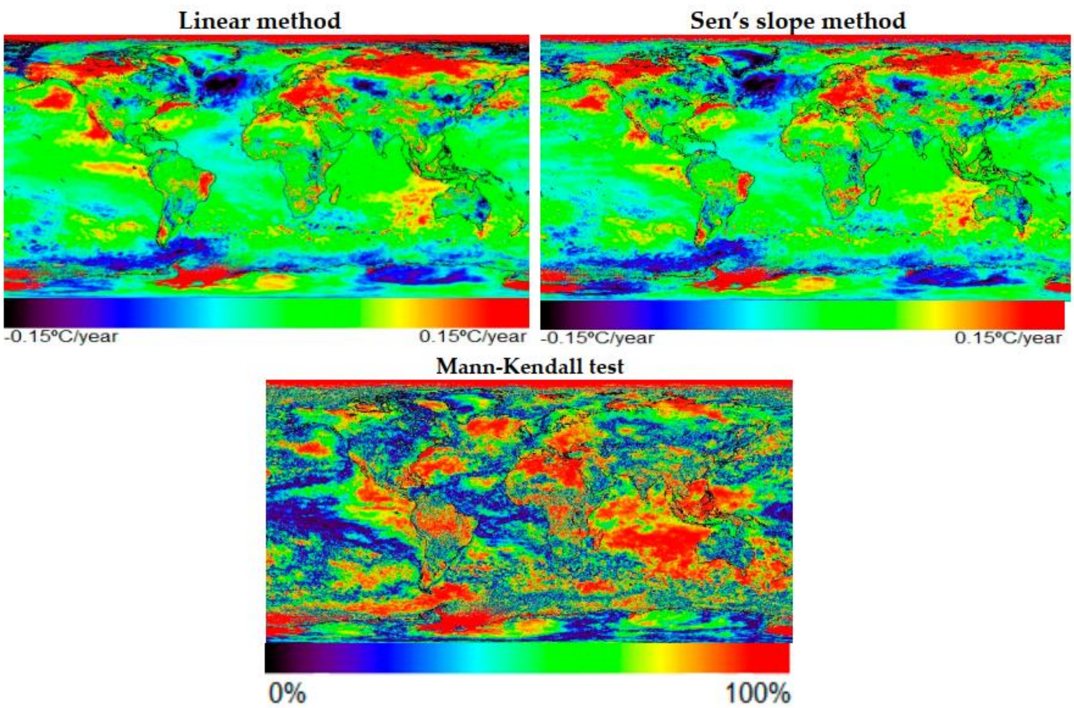

Figure 4. Global linear trend map for the period 2003–2016 estimated by the linear (**left**) and Sen's slope (**right**) methods, with results of 0.018 °C/yr and 0.017 °C/yr, respectively. The Mann-Kendall test significance map is also provided.

Fig. R2. Screenshot of Figure 4 in Sobrino et al. (2020) describing the global LST trend.

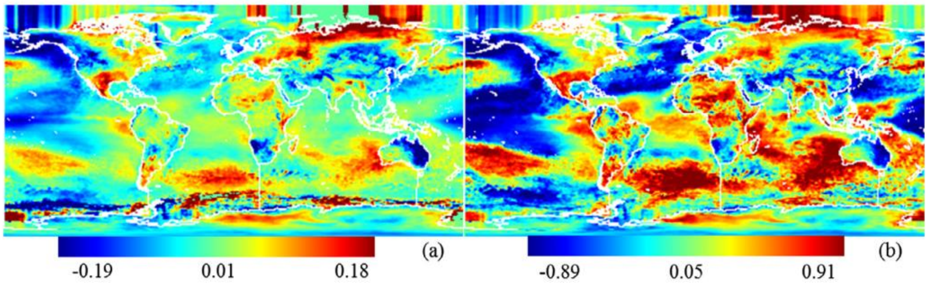

Fig. 5. Global surface temperature change from 2001 to 2012: (a) rate (slope) of linear regression and (b) correlation coefficient.

Fig. R3. Screenshot of Figure 5 in Mao et al. (2017) describing the global LST trend.

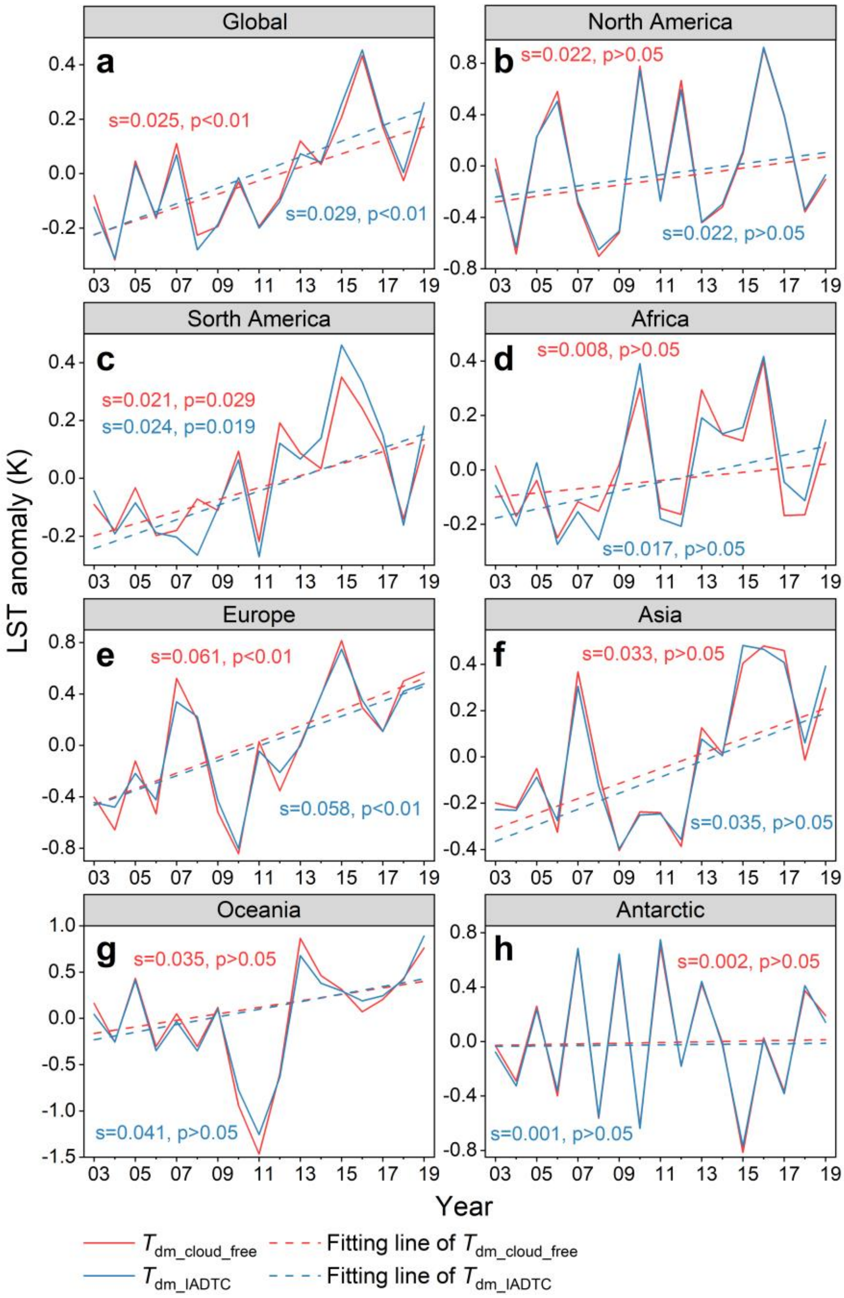

Fig. R4 LST anomalies as well as the associated linear regressions for $T_{dm\_cloud\_free}$ and T_{dm_IADTC} from 2003 to 2019. (**a**) displays the global LST anomalies; and (**b**) to (**h**) display the LST anomalies for each continent.

Comment #9

The threshold determination for the two criteria in Fig. 2 is a little objective. I think the determination can be automatically determined according to the differences between the average value from four observations and the fitted values.

Authors' reply:

Thanks for your comment. Actually, we tried automatically determining the threshold according to the average value from four observations (i.e., $T_{dm\_ATC\_four}$) and the DTC-fitted values (i.e., $T_{dm\_ATC\_DTC}$) when constructing the IADTC framework. We found it hard to design a concise rule to automatically differentiate different scenarios based on the difference between $T_{dm\_ATC\_four}$ and $T_{dm\_ATC\_DTC}$. Therefore, we remain choosing to use the fixed threshold.

We agree with you that there are other strategies to determine the thresholds. Those strategies might achieve better accuracies. However, our current validation results show that simply using the fixed threshold can already achieve satisfactory accuracy.

Comment #10

The LSTs of cloud cover pixels are generated with the reanalysis data at coarse-resolution. Currently, there are some other reconstruction methods without the use of the reanalysis data. How about the applicability of these methods in this study.

Authors' reply:

Thanks for your comment. The role of ATC model is to reconstruct the under-cloud LST with the assistance of reanalysis data. There are some other reconstruction methods without using the reanalysis data, such as statistical interpolation, spatiotemporal fusion, and passive microwave-based method (Wu et al., 2021; Hong et al., 2021). Additionally, previous studies have produced seamless LST datasets (Zhang et al., 2022; Zhao et al., 2020). These methods or products can replace the ATC model in our T_{dm} generation framework. We have clarified this point in Line 547-551, which was given as follows for your convenience.

Line 547-551:

{Third, other high-efficient under-cloud LST reconstruction methods, such as statistical interpolation, spatiotemporal fusion, and passive microwave-based method (Wu et al., 2021; Hong et al., 2021), or the generated under-cloud LST products (Zhang et al., 2022; Zhao et al., 2020), can replace the ATC model in the T_{dm} generation framework. Similarly, more efficient diurnal LST dynamics modelling methods can also replace the DTC model (Jia et al., 2022).}

Comment #11

The dataset produced in this study has the resolution of 0.5 degree. However, to some extent, the LST product at 1-km and higher resolution will be useful. What is the key issue should be addressed at this high-resolution level.

Authors' reply:

Thanks for your comment. We agree with you that 1-km or higher resolution LST products are useful and valuable. Our IADTC framework can be directly applied to the 1-km MODIS LST to generate T_{dm} in a small region. Our previous study provides the example of generating 1-km T_{dm} in Shanghai using the OADTC framework. It can also be generated using the IADTC framework. You can refer to Fig. S1 in (Hong et al., 2021) for more details.

While for generating long-term and large-scale 1-km resolution LST product, calculation efficiency and computation complexity is the key issue. The tons of DTC model fitting using the least-square fitting cover the majority of running time. In the future perspective section, we mentioned three possible ways to reduce the computation complexity and improve the calculation efficiency. The first is to use the similarity of the ATC and DTC model parameters among neighboring pixels to reduce the computation complexity. The second is to combine statistical or empirical estimation strategies to reduce the times of least-square fitting and improve computational efficiency. The third is to use other high-efficient methods to replace the ATC or DTC model in the T_{dm} generation framework. We have provided elaborated descriptions about this point in Line 530-551, which were given as follows for your convenience.

{(2) *Rapid generation of high-resolution spatiotemporally seamless T_{dm} product*: Considering the limited computing resource as well as the aim of this study to obtain the spatial distribution of ΔT_{sb} and LST trends on a global scale, the spatiotemporally seamless daily T_{dm} were generated at a spatial resolution of 0.5 degree. However, current IADTC framework is equally suitable to generate spatiotemporally seamless daily 1-km T_{dm}. For local-scale studies, the IADTC framework can probably be applied directly. While for large-scale (continent-scale or even global-scale) studies or applications, the generation of 1-km spatiotemporally seamless daily T_{dm} could be computationally unaffordable. Under this circumstance, apart from using as many computation resources as possible, we can resort to three strategies to substantially reduce computational complexity.

First, the similarity of the ATC and DTC model parameters among neighboring pixels can be utilized to accelerate the calculation speed considerably (Hong et al., 2021; Hu et al., 2020; Zhan et al., 2016). Second, the physically-based IADTC framework can also be integrated with some statistical or empirical estimation strategies (both on T_{dm} and on ΔT_{sb}) to help improving the computational efficiency (Xing et al., 2021). This is reasonable as ΔT_{sb} (and T_{dm}) is generally related to local surface properties (**Error! Reference source not found.** and **Error! Reference source not found.**). For example, for large-scale or global high-resolution generation of spatiotemporally seamless daily 1-km T_{dm}, the IADTC framework can be run in some chosen sample regions to obtain adequate training samples of T_{dm} (or ΔT_{sb}). Based on these samples, statistical relationships between T_{dm} (ΔT_{sb}) and the related variables such as the four daily LSTs, latitude, land cover type, elevation, and cloud percentage can be obtained to help estimate the T_{dm} (ΔT_{sb}) across the globe efficiently. Furthermore, the training samples of T_{dm} (ΔT_{sb}) can also be from geostationary satellite data, which can help reduce the computational complexity of the DTC modelling. Third, other high-efficient under-cloud LST reconstruction methods, such as statistical interpolation, spatiotemporal fusion, and passive microwave-based method (Wu et al., 2021; Hong et al., 2021), or the generated under-cloud LST products (Zhang et al., 2022; Zhao et al., 2020), can replace the ATC model in the T_{dm} generation framework. Similarly, more efficient diurnal LST dynamics modelling methods can also replace the DTC model (Jia et al., 2022).}

IV. References

Augustine, J. A., DeLuisi, J. J., and Long, C. N.: SURFRAD–A National Surface Radiation Budget Network for Atmospheric Research, Bull. Am. Meteorol. Soc., 81, 2341-2358, doi:10.1175/1520-0477(2000)081%3C2341:SANSRB%3E2.3.CO;2, 2000.

Brown, J. F., Tollerud, H. J., Barber, C. P., Zhou, Q., Dwyer, J. L., Vogelmann, J. E., Loveland, T. R., Woodcock, C. E., Stehman, S. V., Zhu, Z., Pengra, B. W., Smith, K., Horton, J. A., Xian, G., Auch, R. F., Sohl, T. L., Sayler, K. L., Gallant, A. L., Zelenak, D., Reker, R. R., and Rover, J.: Lessons learned implementing an operational continuous United States national land change monitoring capability: The Land Change Monitoring, Assessment, and Projection (LCMAP) approach, Remote Sens. Environ., 238, doi:10.1016/j.rse.2019.111356, 2020.

Cao, S. and Sanchez-Azofeifa, A.: Modeling seasonal surface temperature variations in secondary tropical dry forests, Int. J. Appl. Earth Obs. Geoinf., 62, 122-134, doi:10.1016/j.jag.2017.06.008, 2017.

Duan, S.-B., Li, Z.-L., Li, H., Göttsche, F.-M., Wu, H., Zhao, W., Leng, P., Zhang, X., and Coll, C.: Validation of Collection 6 MODIS land surface temperature product using in situ measurements, Remote Sens. Environ., 225, 16-29, doi:10.1016/j.rse.2019.02.020, 2019.

Ermida, S. L., Soares, P., Mantas, V., Göttsche, F.-M., and Trigo, I. F.: Google Earth Engine open-source code for land surface temperature estimation from the Landsat series, Remote Sens., 12, 1471, doi:10.3390/rs12091471, 2020.

Göttsche, F. M., Olesen, F. S., Trigo, I. F., Bork-Unkelbach, A., and Martin, M. A.: Long term validation of land surface temperature retrieved from MSG/SEVIRI with continuous in-situ measurements in Africa, Remote Sens., 8, doi:10.3390/rs8050410, 2016.

Guillevic, P., Göttsche, F., Nickeson, J., Hulley, G., Ghent, D., Yu, Y., Trigo, I., Hook, S., Sobrino, J., Remedios, J., and Camacho, F.: Land surface temperature product validation best practice protocol. Version 1.1. In P. Guillevic, F. Göttsche, J. Nickeson & M. Román (Eds.), Best practice for satellite-derived land product validation (p. 58): Land product validation subgroup (WGCV/CEOS), doi:10.5067/doc/ceoswgcv/lpv/lst.001, 2018.

Hong, F., Zhan, W., Göttsche, F.-M., Lai, J., Liu, Z., Hu, L., Fu, P., Huang, F., Li, J., Li, H., and Wu, H.: A simple yet robust framework to estimate accurate daily mean land surface temperature from thermal observations of tandem polar orbiters, Remote Sens. Environ., accepted, 2021.

Jia, A., Liang, S., and Wang, D.: Generating a 2-km, all-sky, hourly land surface temperature product from Advanced Baseline Imager data, Remote Sens. Environ., 278, doi:10.1016/j.rse.2022.113105, 2022.

Kalnay, E., Kanamitsu, M., Kistler, R., Collins, W., Deaven, D., Gandin, L., Iredell, M., Saha, S., White, G., Woollen, J., Zhu, Y., Chelliah, M., Ebisuzaki, W., Higgins, W., Janowiak, J., Mo, K. C., Ropelewski, C., Wang, J., Leetmaa, A., Reynolds, R., Jenne, R., and Joseph, D.: The NCEP/NCAR 40-Year Reanalysis Project, Bull. Am. Meteorol. Soc., 77, 437-472, doi:10.1175/1520-0477(1996)077<0437:TNYRP>2.0.CO;2 %J Bulletin of the American Meteorological Society, 1996.

Kobayashi, S., Ota, Y., Harada, Y., Ebita, A., Moriya, M., Onoda, H., Onogi, K., Kamahori, H., Kobayashi, C., Endo, H., Miyaoka, K., and Takahashi, K.: The JRA-55 Reanalysis: General Specifications and Basic Characteristics, Journal of the Meteorological Society of Japan. Ser. II, 93, 5-48, doi:10.2151/jmsj.2015-

001, 2015.

Ma, J., Shen, H., Wu, P., Wu, J., Gao, M., and Meng, C.: Generating gapless land surface temperature with a high spatio-temporal resolution by fusing multi-source satellite-observed and model-simulated data, Remote Sens. Environ., 278, doi:10.1016/j.rse.2022.113083, 2022.

Mao, K. B., Ma, Y., Tan, X. L., Shen, X. Y., Liu, G., Li, Z. L., Chen, J. M., and Xia, L.: Global surface temperature change analysis based on MODIS data in recent twelve years, Adv. Space Res., 59, 503-512, doi:10.1016/j.asr.2016.11.007, 2017.

Muñoz-Sabater, J., Dutra, E., Agustí-Panareda, A., Albergel, C., Arduini, G., Balsamo, G., Boussetta, S., Choulga, M., Harrigan, S., Hersbach, H., Martens, B., Miralles, D. G., Piles, M., Rodríguez-Fernández, N. J., Zsoter, E., Buontempo, C., and Thépaut, J.-N.: ERA5-Land: a state-of-the-art global reanalysis dataset for land applications, Earth System Science Data, 13, 4349-4383, doi:10.5194/essd-13-4349-2021, 2021.

Østby, T. I., Schuler, T. V., and Westermann, S.: Severe cloud contamination of MODIS Land Surface Temperatures over an Arctic ice cap, Svalbard, Remote Sens. Environ., 142, 95-102, doi:10.1016/j.rse.2013.11.005, 2014.

Rodell, M., Houser, P. R., Jambor, U., Gottschalck, J., Mitchell, K., Meng, C.-J., Arsenault, K., Cosgrove, B., Radakovich, J., Bosilovich, M., Entin, J. K., Walker, J. P., Lohmann, D., and Toll, D.: The Global Land Data Assimilation System, Bull. Am. Meteorol. Soc., 85, 381-394, doi:10.1175/BAMS-85-3-381, 2004.

Sobrino, J. A., Julien, Y., and García-Monteiro, S.: Surface temperature of the planet Earth from satellite data, Remote Sens., 12, 218, doi:10.3390/rs12020218, 2020.

Wan, Z. and Li, Z. L.: A physics-based algorithm for retrieving land-surface emissivity and temperature from EOS/MODIS data, IEEE Trans. Geosci. Remote Sens., 35, 980-996, doi:10.1109/36.602541, 1997.

Westermann, S., Langer, M., and Boike, J.: Systematic bias of average winter-time land surface temperatures inferred from MODIS at a site on Svalbard, Norway, Remote Sens. Environ., 118, 162-167, doi:10.1016/j.rse.2011.10.025, 2012.

Wu, P., Yin, Z., Zeng, C., Duan, S.-B., Gottsche, F.-M., Ma, X., Li, X., Yang, H., and Shen, H.: Spatially continuous and high-resolution land surface temperature product generation: A review of reconstruction and spatiotemporal fusion techniques, IEEE Geoscience and Remote Sensing Magazine, 9, 112-137, doi:10.1109/mgrs.2021.3050782, 2021.

Zhang, T., Zhou, Y., Zhu, Z., Li, X., and Asrar, G. R.: A global seamless 1 km resolution daily land surface temperature dataset (2003–2020), Earth System Science Data, 14, 651-664, doi:10.5194/essd-14-651-2022, 2022.

Zhang, X., Zhou, J., Liang, S., Chai, L., Wang, D., and Liu, J.: Estimation of 1-km all-weather remotely sensed land surface temperature based on reconstructed spatial-seamless satellite passive microwave brightness temperature and thermal infrared data, ISPRS J. Photogramm. Remote Sens., 167, 321-344, doi:10.1016/j.isprsjprs.2020.07.014, 2020.

Zhao, B., Mao, K., Cai, Y., Shi, J., Li, Z., Qin, Z., Meng, X., Shen, X., and Guo, Z.: A combined Terra and Aqua MODIS land surface temperature and meteorological station data product for China from 2003 to 2017, Earth System Science Data, 12, 2555-2577, doi:10.5194/essd-12-2555-2020, 2020.